ACCSCIENCE PUBLISHING

International Journal of Bioprinting

RESEARCH ARTICLE

3D-bioprinted cell-laden blood vessel with dual drug delivery nanoparticles for advancing vascular regeneration

Eun Ji Lee[1,2†], Jaewoo Choi[1,2†], Hye Ji Lim[1,2], Deokhyeon Yoon[1,2], Dong Myoung Lee[1,2], Donggu Kang[3], Jeong-Seok Lee[3], Hojun Jeon[3], Kyeong Hyeon Lee[4], Yong-Il Shin[4,5], Sang-Cheol Han[6], Woong Bi Jang[1,2*], and Sang-Mo Kwon[1,2*]

[1]Laboratory for Vascular Medicine and Stem Cell Biology, Department of Physiology, Medical Research Institute, School of Medicine, Pusan National University, Yangsan, Republic of Korea

[2]Convergence Stem Cell Research Center, Pusan National University, Yangsan, Republic of Korea

[3]Research Institute of Additive Manufacturing and Regenerative Medicine, Baobab Healthcare Inc., 55 Hanyangdaehak-Ro, Ansan, Gyeonggi-do, South Korea

[4]Science of Convergence, School of Medicine, Pusan National University, Yangsan, Republic of Korea

[5]Department of Rehabilitation Medicine, Pusan National University Yangsan Hospital, Yangsan, Republic of Korea

[6]CEN Co., Ltd., Nano-Convergence Center, 761 Muan-ro, Miryang, Republic of Korea

(This article belongs to the *Special Issue: Nano-enabled 3D Bioprinting for Various Tissue Engineering*)

Abstract

Vascular regeneration plays a critical role in the treatment of cardiovascular diseases and in tissue engineering applications. In this study, we fabricated and characterized statin/curcumin-loaded nanoparticles for potential applications in vascular regeneration. The nanoparticles exhibited consistent spherical shape and sizes, indicating reproducibility and stability of the fabrication process. The sustained release of the loaded drugs from the nanoparticles indicated their suitability for controlled and prolonged drug delivery. Biocompatibility assessments revealed that the nanoparticles were nontoxic even at high concentrations and over extended periods. Moreover, the incorporation of statin within the nanoparticles enhanced the proliferative capacity and functional abilities of endothelial progenitor cells, thereby promoting angiogenesis and vascular repair. Co-administration of curcumin with statin further augmented the therapeutic effects by reducing intracellular reactive oxygen species levels and providing antioxidant protection against oxidative stress. Furthermore, we successfully integrated these nanoparticles into artificial blood vessels (ABVs) using three-dimensional printing technology, creating customizable constructs capable of supporting vascular regeneration. The viability and proliferative capacity of cells within the ABVs were preserved, which has potential for targeted drug delivery and localized therapy. In *in vivo* models of hindlimb ischemia, transplantation of nanoparticle-loaded ABVs resulted in significant improvements in terms of recovery speed and blood flow. Histological analysis confirmed the enhanced expression of vascular-related markers, indicating improved angiogenesis. Collectively, our findings demonstrate the potential of statin/curcumin-loaded nanoparticles as a promising approach for vascular tissue engineering and regenerative medicine. These nanoparticles offer controlled drug delivery, biocompatibility, and enhanced regenerative properties, suggesting that

†These authors contributed equally to this work.

***Corresponding authors:**
Woong Bi Jang
(jangwoongbi@naver.com)

Sang-Mo Kwon
(smkwon323@pusan.ac.kr)

Citation: Lee EJ, Choi J, Lim HJ, et al. 3D-bioprinted cell-laden blood vessel with dual drug delivery nanoparticles for advancing vascular regeneration. *Int J Bioprint.* 2024;10(2):1857.
doi: 10.36922/ijb.1857

Received: September 18, 2023
Accepted: November 17, 2023
Published Online: January 12, 2024

they are valuable tools for promoting vascular regeneration and advancing therapeutic interventions for cardiovascular diseases. Further research is required to fully elucidate the mechanisms of action and optimize their clinical applications.

Keywords: 3D Bioprinting; Nanoparticles; Artificial blood vessels; Atorvastatin; Curcumin

1. Introduction

Vascular diseases encompass a wide variety of conditions affecting blood vessels and present significant challenges to modern healthcare. From atherosclerosis to peripheral arterial disease, these disorders can lead to severe complications and increase the risk of life-threatening events such as heart attack and stroke.[1-5] Thus, there is a growing need for innovative approaches that can address these conditions more effectively and provide novel methods for treatment and prevention.[6-8] Traditional treatment methods, such as drugs, aim to prevent or manage vascular diseases by strengthening blood vessel function, lowering blood pressure, and preventing blood clot formation. Although these approaches offer preventive benefits, they do not provide a comprehensive treatment strategy for vascular diseases.[9-12] Surgical interventions, including the use of stents, catheters, and artificial blood vessels (ABVs), are often performed in severe cases of vascular diseases. These interventions can deliver immediate therapeutic efficacy by improving the blood flow. However, they have some limitations. Issues such as restenosis (re-narrowing of the blood vessels) after surgery and the challenge of fully restoring non-functional blood vessels limit their long-term effectiveness.[13-16] The emergence of cell therapy products as next-generation treatment strategies holds promise for addressing the limitations of traditional approaches. Cell therapies aim to utilize cells that can repair damaged blood vessels and promote the formation of new blood vessels.[17-20] However, current cell therapies face challenges related to limited cell transplantation ability and the capacity for multipotent angiogenesis (the formation of new blood vessels from pre-existing ones).[21-23]

Among the available approaches, ABVs have been the focal point of research within the medical field, with a primary objective of evaluating and enhancing their performance and safety compared to natural vessels. These ABVs come in various types, including synthetic versions typically composed of thermosensitive polymers and biological constructs crafted from actual tissues. The advantages of ABVs include customization for individual patients, cost-effectiveness in some cases, and compatibility for transplantation. However, the application of ABVs is limited by the risk of infection and potential endothelial cell deficiencies in synthetic variants. Ongoing research strives to overcome these limitations, aiming to improve the utility and safety of artificial blood vessels in medical applications.[24-27] An innovative approach that combines drugs, ABVs, surgical interventions such as stents or catheters, and cell therapies to achieve maximum efficiency by accentuating their respective strengths and while overcoming their weaknesses is garnering increasing attention.[28-30] Prior to the inception of three-dimensional (3D) printing technology, the concept of utilizing combination therapy of drugs and cells in vascular disorder treatments prevailed.[31-33] The technological advancements in 3D printing have led to significant progress in the development of ABVs loaded with cells. Blood vessels consist of various cell types and multiple layers. The transplantation of 3D-printed ABVs alone is fraught with limitations in terms of durability, performance, and regenerative capacity compared to natural blood vessels.[34-36] To address these limitations, cell incorporation is executed during the production of ABVs to heighten their resemblance to native tissue so as to enhance blood vessel regeneration and improve their compatibility.[37-39] For this reason, studies on printing cells loaded with drugs to improve cell functions have been conducted.[40-43] However, maximizing the therapeutic efficacy of transplanted ABVs remains challenging.

Transplantation for ischemic diseases triggers substantial alterations in the surrounding microenvironment. These changes stem from various factors, including diminished oxygen levels resulting from blood loss during the transplantation process under ischemic conditions.[44-46] Additionally, the induction of inflammation and immune responses within the microenvironment occurs as immune cells are recruited to the transplant site, leading to heightened oxidative stress.[45,47,48] These factors collectively impact tissue damage and cellular interactions within the microenvironment. Understanding these intricate microenvironmental alterations is imperative to facilitate the recovery process following transplant surgery in ischemic diseases. Among these dynamic changes, the increased level of reactive oxygen species (ROS) is the prime issue to tackle with. During transplantation, the graft may experience ischemia-reperfusion injury, a condition where the blood supply to the graft is temporarily reduced (ischemia) and then restored when it is connected to the

recipient's circulatory system (reperfusion). This abrupt change in oxygen supply can trigger the production of ROS.[49-51] Additionally, the inflammatory response and immune reactions against the graft contribute to elevated ROS levels, as immune cells generate ROS as part of their defense mechanisms.[48,52,53] Moreover, surgical trauma and tissue manipulation during the transplantation process can disrupt the tissue's natural antioxidant defenses, further promoting oxidative stress. Despite the remarkable effectiveness of ABVs, cells often struggle to adapt to the ROS or hypoxic environment at transplant sites.[54-56] This limitation hinders the translation of their superior efficacy into clinical applications. Therefore, understanding and managing ROS levels during transplantation are of paramount importance to enhance graft survival and overall transplant outcomes.

Curcumin, which enhances the antioxidant and anti-inflammatory responses of cells, has been used to help cells adapt to the microenvironment.[57-59] In this study, we combined curcumin with statin to enhance cell function. Statins, commonly prescribed to lower cholesterol levels, have shown remarkable protective effect on cardiovascular system by reducing plaque formation and inflammation within blood vessels. When statin is applied to endothelial progenitor cells, it enhances nitric oxide production for vasodilation, promotes cell differentiation and maturation, suppresses inflammation, and fosters vascular growth. These mechanisms collectively safeguard vascular health by improving function, promoting restoration, and ensuring endothelial integrity.[60-62]

Cutting-edge nanotechnological techniques have been employed to optimize the delivery and effectiveness of statins and curcumin. While loading two different drugs, the difference in molecular weights and size polarity gives rise to a problem in merging and processing. Encapsulating these substances within nanoparticles has several advantages, including enhanced bioavailability, controlled release, similar characteristics, and targeted delivery. This nanoparticle-based approach not only improves the efficiency of the drug achieved with slow, sustained release of the drug, but also minimizes potential side effects.[63-67] The integration of these advanced techniques seeks to overcome the limitations of the existing treatment methods. Previous investigations were conducted utilizing ABVs and statin-loaded nanoparticles. However, ABVs and statin in isolation present certain limitations. To address these limitations, we encapsulated the drug within nanoparticles and subsequently loaded these nanoparticles into an ABV to validate the efficacy.[68] By combining the benefits of nanoparticle function-enhancing substances, nanoparticles loaded with antioxidant and anti-inflammation substances, stem cells, and 3D printing, it is anticipated that the fundamental challenges of vascular diseases, including the restoration of blood vessel functionality and promotion of angiogenesis, can be addressed more effectively.

2. Materials and methods

2.1. Preparation of nanoparticles, statin-loaded nanoparticles, and curcumin-loaded nanoparticles

Nanoparticles were synthesized using a modified version of a previously reported method.[69] In this procedure, 0.5 g of cetyltrimethylammonium bromide (CTAB) was dissolved in 1000 mL of deionized water, and 2 mL of 1 M NaOH was added with continuous stirring. Next, 1 mL of tetraethyl orthosilicate (TEOS) and 0.1 g of N-(2-aminoethyl)-3-aminopropyltrimethoxy silane (AEAPTMS) were separately dissolved in ethanol in a 1:5 volume ratio and 1:5 weight ratio, respectively, and added to the solution. The resulting mixture formed a white precipitate, which was filtered, washed, and dried at 80°C for 48 h. To remove CTAB, the dried precipitate was dispersed in 100 mL of ethanol, and 0.3 g of NH_4NO_3 was added to the solution. The mixture was stirred at 60°C for several hours, and the precipitate was filtered out and dried at 60°C for 12 h. Subsequently, 0.2 g of $ZnCl_2$ was dissolved in deionized water, and the obtained precipitate was added to the zinc solution. The solution was then dried using a rotary evaporator. The resulting powder was further processed by centrifugation, followed by multiple washes with water and ethanol, drying at 80°C for 12 h, and finally calcination at 55°C for more than 5 h. This product was labeled as nanoparticle (NP). To prepare statin-loaded nanoparticle (NPS) and curcumin-loaded nanoparticle (NPC), 80 mg of NP was dissolved in 80 mL of ethanol and dispersed with ultrasonic waves for 3 min. Simultaneously, 20 mg of statin and curcumin were dissolved in 20 mL of ethanol and mixed at 300 rpm for 3 min. The two solutions were then depressurized under vacuum for 1 h at a pressure of 100 bar. Subsequently, the pressure was lowered to 60 bar and maintained for 30 min before the sample was dried under vacuum at room temperature for 6 h. The resulting products containing statin and curcumin were denoted as NPS and NPC, respectively.

2.2. Characterization of particle size, polydispersity, and composition

Electron microscopy was conducted to qualitatively assess the size and polydispersity of NP, NPS, and NPC. While preparing sample for bio-transmission electron microscope (Bio-TEM; Talos L120C TEM, Thermo Fisher Scientific, Carlsbad, CA, USA), 100 μL of the particles sample in deionized water was dropped on copper grid (FCF200-

CU-50, Electron Microscopy Sciences, USA), and the grid was dried at room temperature at 24 h. All images were recorded using a Gatan 4k × 4k Thermo Scientific Ceta CMOS. The dimensions of the images acquired within each grid were quantified using the ImageJ analysis program and visually represented through a size distribution graph. While preparing sample for transmission electron microscope-energy dispersive spectrometer (TEM-EDS; Talos F200X, Thermo Fisher Scientific, Carlsbad, CA, USA), 100 µL of the particles sample in methanol was dropped on copper grid (FCF200-CU-50, Electron Microscopy Sciences, USA) and washed with deionized water twice. To observe the sample, the grid was dried at room temperature for 24 h. The composition of rapamycin, NP, and NPR was analyzed with Fourier transform infrared (FTIR) spectroscopy. The FTIR spectra of the samples were generated by Nicolet 560 FTIR spectroscope (Nicolet Co., Madison, WI, USA) with 4.0 cm^{-1} resolution and 16 scans ranging from 4000 to 750 cm^{-1}.

2.3. Zeta potential analysis of NP, NPS, and NPC

The zeta potential in NP, NPS, and NPC was measured using Zetasizer Nano ZS (Malvern Instruments). The evaluation of zeta potential was performed based on the principle of electrophotoretic light scattering. A dip cell (zen1002, Malvern Instruments, Malvern, UK) with a pair of parallel palladium electrodes was used to provide electrical trigger on charged particles. The experiments were performed in triplicate, and the data were analyzed using Zetasizer Software.

2.4. Determination of drug release

We prepared calibration standard solutions by diluting NPS and NPC in distilled water, yielding the first standard solution of 10 mg/mL, which was further diluted with methanol to final concentrations of 10, 50, and 100 ppb. The samples were prepared by diluting and soaking NPS and NPC in distilled water, yielding solutions at a concentration of 1 mg/mL, for 7 days prior to releasing. The released samples were filtered with a pore filter (pore size: 0.22 µm). The filtered solution was centrifuged at 10,000 × g for 10 min, and the supernatant was diluted with methanol to a final concentration of 0.01 mg/mL. QTRAP 6500 + low-mass liquid chromatography/mass spectrometry (LC/MS) system (SCIEX, Canada) was used to analyze the cumulative release of NPS and NPC.

2.5. Isolation of endothelial progenitor cells and cell culture

Human endothelial progenitor cells (EPCs) were isolated from human umbilical cord blood as previously described.[70] Briefly, human umbilical cord blood was collected from healthy volunteers after obtaining informed consent according to the protocol approved by the Institutional Review Board of Pusan National University Yangsan Hospital, Republic of Korea (Approval No. PNUYH-05-2017-053). Total mononuclear cells were isolated with Ficoll (GE Healthcare, Buckinghamshire, UK) gradient density centrifugation of human umbilical cord blood. Freshly isolated cells were cultured in endothelial growth medium-2 (EGM-2) supplemented with 5% fetal bovine serum (FBS), human vascular endothelial growth factor (VEGF), human basic fibroblast growth factor, human epidermal growth factor, human insulin-like growth factor 1, ascorbic acid, and GA-1000 (Lonza, Walkersville, MD, USA). The cultures were maintained at 37°C in a 5% CO_2 humidified atmosphere. After 4 days of culture, non-adherent cells were discarded, and the attached cells were further cultured. The cells were subjected to long-term culture to allow the formation of spindle-shaped colonies, and the medium was replenished every 14–21 days. Flow cytometric analysis performed to characterize several surface and pivotal functional markers confirmed that the EPCs were positive for endothelial lineage markers (CD31 and VEGFR2) and hematopoietic stem cell markers (CD34, CXCR4, and c-Kit), and negative for hematopoietic markers such as CD11b, CD14, and CD45.

2.6. Cell viability assay

The viability assay for EPCs was conducted using a cell counting kit-8 (CCK-8) (Dongin, CCK-3000, Seoul, Republic of Korea), according to the manufacturer's instructions. For the analysis of cell toxicity, 5000 cells/well were seeded into each 96-well plate, the medium was replaced with fresh medium containing NP, NPS, and NPC at various concentrations, and the cells were incubated for 24, 48, and 72 h. After incubation, the medium was replaced with 100 µL of 1:10 diluted CCK-8 solution. The plates were then incubated for an additional 1 h. Absorbance was measured at 450 nm using a spectrophotometer (TECAN, Grodig, Austria). Each experiment was repeated at least three times.

2.7. Proliferation assay

To evaluate the proliferation of EPCs, Click-iT® Plus EdU Alexa Fluor® 488 Imaging Kit (C10637; Thermo Fisher Scientific) that uses modified 5-ethynyl-2'-deoxyuridine (a nucleoside analog of thymidine), which can be efficiently incorporated into newly synthesized DNA, was used. For the analysis of cell proliferation, 10,000 cells/well were seeded into each 8-well chamber (154534, Thermo Fisher Scientific, Carlsbad, CA, USA) and pre-conditioned with NP, NPS, and NPC in EGM-2 media for 24 h. The samples were incubated for 2 h in EdU solution and processed according to the manufacturer's instructions. The labeling index was evaluated as EdU-labeled nuclei relative to 4',6-diamidino-2-phenylindole (DAPI)-stained nuclei.

2.8. Tube formation assay

Tube formation assay was performed to assess the function of EPCs in the formation of blood vessel-like structures (tubes). 96-well plates were coated with 65 μL of Matrigel (BD Biosciences, San Diego, CA) and incubated at 37°**C** for 30 min. Afterward, 5000 cells were seeded into each well of a Matrigel-coated 96-well plate. After a 3-h incubation, the plate was examined every hour for tube formation. The total tube length was measured using ImageJ software.

2.9. Migration assay

Migration assay was performed using a 24-well 8.0 μm polycarbonate Transwell chamber consisting of a permeable membrane (Corning Inc., Corning, NY, USA). For the assay, 500 μL of EGM-2 media was added below the cell permeable membrane, while 10,000 cells/100 μL in EBM-2 medium were plated on the upper chamber of the permeable membrane. After 24 h of incubation, the migrated cells were fixed with 4% paraformaldehyde and stained with 0.5% crystal violet at room temperature. The upper chamber was washed, and the top of the membrane was examined for cell migration. The cells were observed under an inverted microscope after mounting, and the number of cells was counted.

2.10. Measurement of intracellular ROS levels

Intracellular ROS levels were measured using the 2′,7′-dichlorodihydrofluorescein diacetate (H_2DCFDA) kit (Thermo Fisher Scientific, Carlsbad, CA, USA). After incubation, the EPCs were harvested and washed with 2% FBS and 200 μM ethylenediaminetetraacetic acid (EDTA) in PBS. After centrifugation at 2000 ×g for 3 min, the pellet was suspended in 10 μM H_2DCFDA in PBS containing 2% FBS and 200 μM EDTA and incubated for 1 h at 37°C in 5% CO_2 atmosphere. Following which, the cells were washed with PBS and analyzed by flow cytometry using the BD Accuri C6 software (BD Biosciences, New Jersey, USA).

2.11. Preparation and mechanical property evaluation of 3D-bioprinted artificial blood vessel

To prepare bioinks, sodium alginate (viscosity >2000 cP, 25°C; Sigma-Aldrich, St. Louis, MO, USA) in Dulbecco's phosphate-buffered saline (DPBS, Gibco, Grand Island, USA) was prepared and stirred for 6 h at 37°C. Next, an atelocollagen solution (pH 4.0; Baobab Healthcare, Gyeonggi-do, Republic of Korea) was mixed with reconstituted buffer (132 mM Na_2HPO_4) at a volume ratio of 1:1 for neutralization.

Vascular printing was performed using a coaxial nozzle (inner needle, 28 G; outer needle, 20 G; Ramé-hart, Succasunna, NJ, USA) equipped with a 3D bioprinter (Root 1; Baobab Healthcare, Gyeonggi-do, Republic of Korea). For the shell material, bioinks were prepared by combining 3% w/v neutralized atelocollagen and 3% w/v alginate at a 4:1 ratio. NPS and NPC (6 mg/500 μL each) were then blended with the shell bioinks (3 mL), resulting in a final concentration of 2 mg/mL for both NPS and NPC in the bioink. Similarly, NP was mixed with the shell bioink as the control group. For the core material, 40% w/v Pluronic F-12 (Sigma-Aldrich) with 100 mM calcium chloride was used as the sacrificial material. For vascular cell printing, the shell material was blended with EPCs (1×10^6 cells/mL). NP, NPS, and NPC without cells were used as controls. The core-shell bioinks were bioprinted at 80 kPa (core) and 60 kPa (shell) using a 200 mM $CaCl_2$ solution to enable *in situ* crosslinking of the alginate solution. Subsequently, the printed vessel was rinsed with DPBS and incubated at 37°C for 1 h. The sacrificial material (core bioink) was removed using ice-cold DPBS. One side of the ABV was set to circulate water with the aid of a circulation pump (MasterFlex L/S, Masterflex, Germany), while the other side was attached to a digital pressure gauge to measure the burst pressure of the ABV. The burst pressure was measured at the point right before ABV rupture, and the burst pressure of cell-laden ABV was measured after 7 days of cultivation.

2.12. Live/dead cell assay

Calcein acetoxy methylester (calcein AM) and ethidium homodimer-2 (InvitrogenTM Life Technologies, Carlsbad, CA, USA) dissolved in 1× PBS, at the concentration of 4 μM and 2 μM, respectively, were used. Calcein AM labels living cells with bright green fluorescence, while ethidium homodimer is a red fluorophore that stains nonviable cells since it cannot penetrate living cells. After 15 min of incubation, the samples were analyzed using a Lionheart FX automated microscope (BioTek, Winooski, VT, USA).

2.13. Fluidity test on artificial blood vessels

To assess the perfusion and patency of a 3D-printed ABV, perfusion test was conducted using pigment ink. The ABV was cut to an appropriate length, and a continuous flow of pigment ink was introduced into the vessel using a 26 G (1/2 inch) syringe. Then, the diffusion of pigment was observed.

2.14. Western blotting

Total protein was isolated from ABV using RIPA Buffer (Thermo Fisher Scientific, Waltham, MA, USA) and a protease inhibitor (Thermo Fisher Scientific, Waltham, MA, USA), according to the manufacturer's specifications. Equal amounts of protein were separated by an 8–15% sodium dodecyl sulfate polyacrylamide gel electrophoresis (SDS-PAGE). The protein bands were then transferred to a polyvinylidene fluoride (PVDF) membrane (Millipore, Billerica, MA, USA). After the membrane was blocked in 5% skim milk for 1 h at room temperature, it was incubated overnight at 4°C with primary antibodies for VE-cadherin,

Ki-67, and β-actin. After incubation with the secondary antibody, i.e., goat anti-rabbit IgG-HRP (ADI-SAB-100-J, Enzo Life Sciences, USA), the bands were visualized using Luminate Crescendo Western HRP Substrate (Millipore, Billerica, MA, USA) and an X-ray film. β-actin was used as the loading control for Western blotting experiment.

2.15. Mouse model of hindlimb ischemia

BALB/c (Nu/Nu) athymic immunodeficient mice unable to produce T cells were used as the animal model of hindlimb ischemia in which transplantation of 3D-printed bio-vessel was performed. BALB/c (Nu/Nu) mice (average weight: 20–24 g) were purchased from Orient Bio (Seongnam, Gyeonggi, Republic of Korea). All animals were housed in an air-conditioned animal room with constant relative humidity and were given access to standard food and water. Animal treatment and maintenance were performed in accordance with the Principles of Laboratory Animal Care, and animal experiments were performed in accordance with the protocols approved by the Pusan National University Institutional Animal Use and Care Committee (Approval No. PNU-2022-0212). All mice were anesthetized by an intraperitoneal injection of 400 mg/kg 2,2,2 tribromoethanol (Avertin; Sigma-Aldrich) prior to the surgical resection of femoral artery and laser Doppler perfusion imaging. The femoral artery was excised from its proximal origin at the branch of the external iliac artery to the distal point, where it bifurcated into the saphenous and popliteal arteries. Immediately after arterial ligation, ischemic hind limbs were transplanted with PBS, EPC, NP@BV (NP-loaded blood vessel), EPC@NP@BV (blood vessel loaded with EPC and NP), and EPC@NPSC@BV (blood vessel loaded with EPC, NPS, and NPC).

2.16. Measurement of blood perfusion and necrosis

Angiogenesis in mouse model with hindlimb ischemia was examined with laser Doppler perfusion imaging (LDPI; Moor Instruments Ltd, Devon, UK) at four time points: 0, 3, 7, 14, and 28 days post-induction of hindlimb ischemia. The blood perfusion levels were measured by comparing the normal right hind limb with the ischemic left hind limb at each time point. The data obtained from LDPI were analyzed using the moorLDI program, a specialized software for assessing blood flow and angiogenesis in preclinical studies. Necrosis was assessed in mice at 0 and 14 days after hindlimb ischemia induction. The extent of necrosis occurring in each animal was quantitatively measured.

2.17. Histological and immunofluorescence analyses

To perform immunostaining, the acquired hindlimb muscles were formalin-fixed, paraffin-embedded, and sectioned at 5 μm. Blood vessels were stained with antibodies for alpha smooth muscle actin (ab5694, 1:100; Abcam plc., Cambridge, UK) and CD31 (ab28364, 1:100; Abcam plc., Cambridge, UK). At first, the paraffin was melted, and the slides were washed using xylan and ethanol. Following antigen retrieval, the tissue was reacted in blocking buffer for 1 h, and the primary antibody was incubated overnight at 4°C. The specimens were incubated with Alexa Fluor 488 secondary antibodies and Alexa Fluor 594 secondary antibodies (Thermo Fisher Scientific, Carlsbad, CA, USA) for 2 h and then washed three times. Nuclei was stained with DAPI using ProLong Diamond Antifade Mountant with DAPI (Invitrogen). Stained sections were visualized using a Lionheart FX automated microscope (BioTek, Winooski, USA).

2.18. Dihydroethidium staining

Before staining with dihydroethidium (DHE; D7008, Sigma-Aldrich, Saint Louis, MO, USA), the tissue sections were rinsed with PBS and incubated with 5 mM DHE for 30 min at 37°C. Stained sections were viewed under Lionheart FX automated microscope (BioTek, Winooski, USA). The percentage of the area exhibiting DHE-positive staining out of the entire stained area was calculated.

2.19. Statistical analysis

Two-tailed unpaired Student's *t*-test and one-way analysis of variance (ANOVA) were conducted for data analyses using GraphPad Prism software (GraphPad, Inc., La Jolla, CA, USA). Data are expressed as mean ± standard deviation. Differences were considered statistically significant at $p < 0.05$.

3. Results

3.1. Fabrication and characterization of NPS and NPC

In this study, we present the design of 3D-printed artificial blood vessels loaded with nanoparticles, each containing two distinct types of drugs. Atorvastatin and curcumin were individually encapsulated within nanoparticles (Figure 1A and B). Subsequently, 3D-printed artificial blood vessels were fabricated by fusing EPCs, bioink, and nanoparticles (Figure 1C). The resulting engineered vessels were then implanted into a mouse model of hindlimb ischemia (Figure 1D).

Statin and curcumin, as a drug for functional enhancement and as an antioxidant drug, respectively, were loaded onto the nanoparticles. Characterization of pure nanoparticles (NP), NPS, or NPC was performed. Morphological analysis revealed that these nanoparticles were round in shape, and the sizes were constant for NP (282.09 nm), NPS (266.56 nm), and NPC (283.25 nm) (Figure 2A and B). Furthermore, for a more detailed characterization of NP structure, a mapping image was obtained through transmission electron microscope-energy dispersive spectrometer analysis (**Figure S1A** in

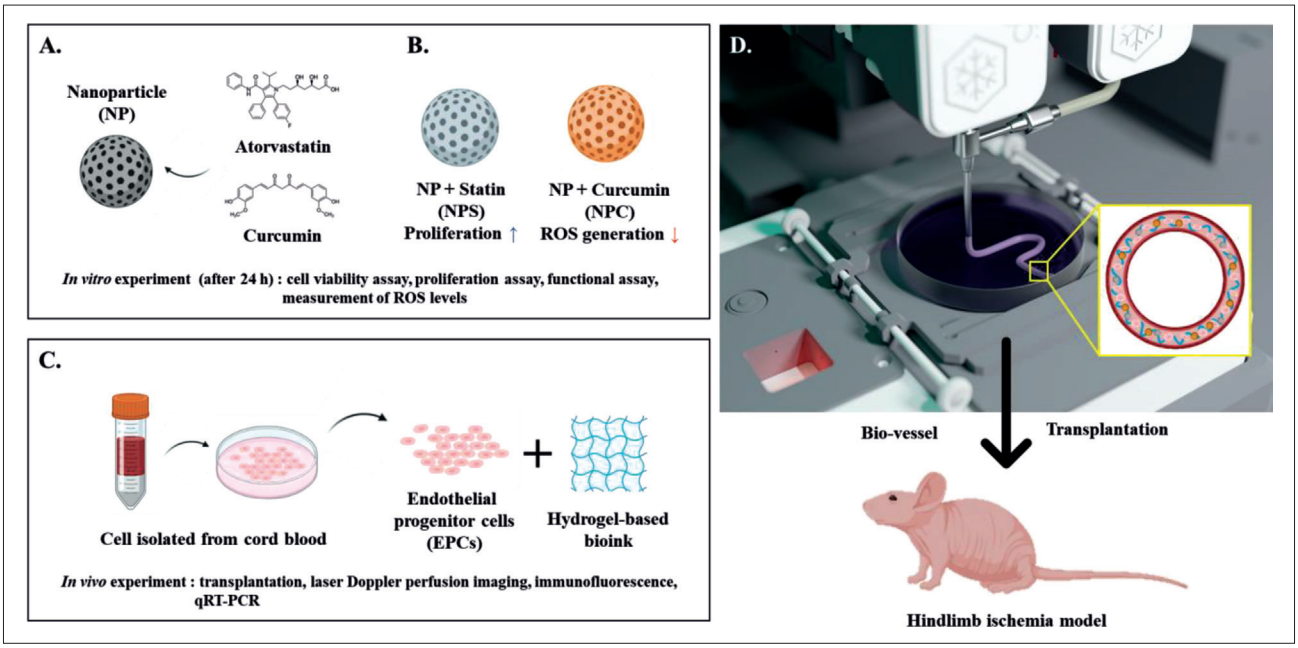

Figure 1. Design of 3D-printed artificial blood vessels (ABVs) loaded with endothelial progenitor cells (EPC) and nanoparticles containing statin and curcumin for treatment in mouse model of hindlimb ischemia. (A) Encapsulation of atorvastatin and curcumin into nanoparticles. (B) Effects of encapsulated NPS and NPC. (C, D) EPCs isolated from umbilical cord blood are combined with bioink to create an ABV, which is transplanted into a mouse model of hindlimb ischemia.

Supplementary File). The analysis confirmed that NP is primarily composed of silicon (Si), oxygen (O), and a trace amount of zinc (Zn). Further quantification of element content revealed approximate weight percentages of 43.9% Si, 53.5% O, and 2.6% Zn, and atomic percentages of 31.6% Si, 67.6% O, and 0.8% Zn (**Figure S1B** and **S1C** in Supplementary File). Based on previous data, NP, NPS, and NPC were individually characterized using FTIR spectroscopy (**Figure S1D** and **S1E** in Supplementary File). In the FTIR spectrum of NP, the presence of a symmetric stretching vibration peak at 1078 cm^{-1} was indicative of the Si-O-Si group, a characteristic feature of SiO_2.[71,72] NPS and NPC exhibited similar characteristics, with Si-O-Si wavelengths observed at 1082 cm^{-1} and 1066 cm^{-1}, respectively. This observation strongly suggests that the primary constituent of NP is SiO_2. NP characterized by this structural configuration demonstrate a loading efficiency of approximately 20% for both statin and curcumin. Zeta potential is often used as an indicator to assess the stability of a sample dispersion. The zeta potential of -16.6 mV for NP, -18.6 mV for NPS, and -20.7 mV for NPC confirmed the stability of the suspension (Figure 2C). To evaluate stability *in vivo*, the degradability of the nanoparticles was evaluated after suspension in PBS, which showed that the shape and size of the nanoparticles were maintained from days 1, 3, and 7 (Figure 2D and E). Subsequently, we performed an experiment to ascertain the quantity of drug released from the NP. Drug release conditions were established with a maximum standard of 7 days (100%), and the daily release rate was then determined. The outcome revealed a slow release of each drug loaded within the nanoparticles (Figure 2F). Overall, it was confirmed that the shape and size of each manufactured nanoparticle were constant and that the content was released from the nanoparticles in a slow but sustained manner.

3.2. *In vitro* biocompatibility assessment of NP

To confirm the cytotoxicity of the nanoparticles, the treatment was performed for each concentration and time period (Figure 3A). No cytotoxicity was observed even when the cells were treated at a high concentration of 1 μg/mL for up to 72 h (Figure 3B). Besides, we found that EPCs treated with NPS demonstrated enhanced proliferation and function. When NPS and NPC (NPSC) were co-administered, a similar tendency was observed (Figure 3C). EdU assay was performed to confirm whether this result was due to an increase in the number of proliferating cells. It was confirmed that the NP was nontoxic, and the number of proliferating cells significantly increased when treated with NPSC (Figure 3D and E). To establish the additional role of statin in enhancing the functions of EPCs, an experiment was conducted to assess blood vessel formation and migration ability. It was confirmed that tube formation (Figure 3F and G) and migration (Figure 3H and I), which are the indicators of angiogenesis, were

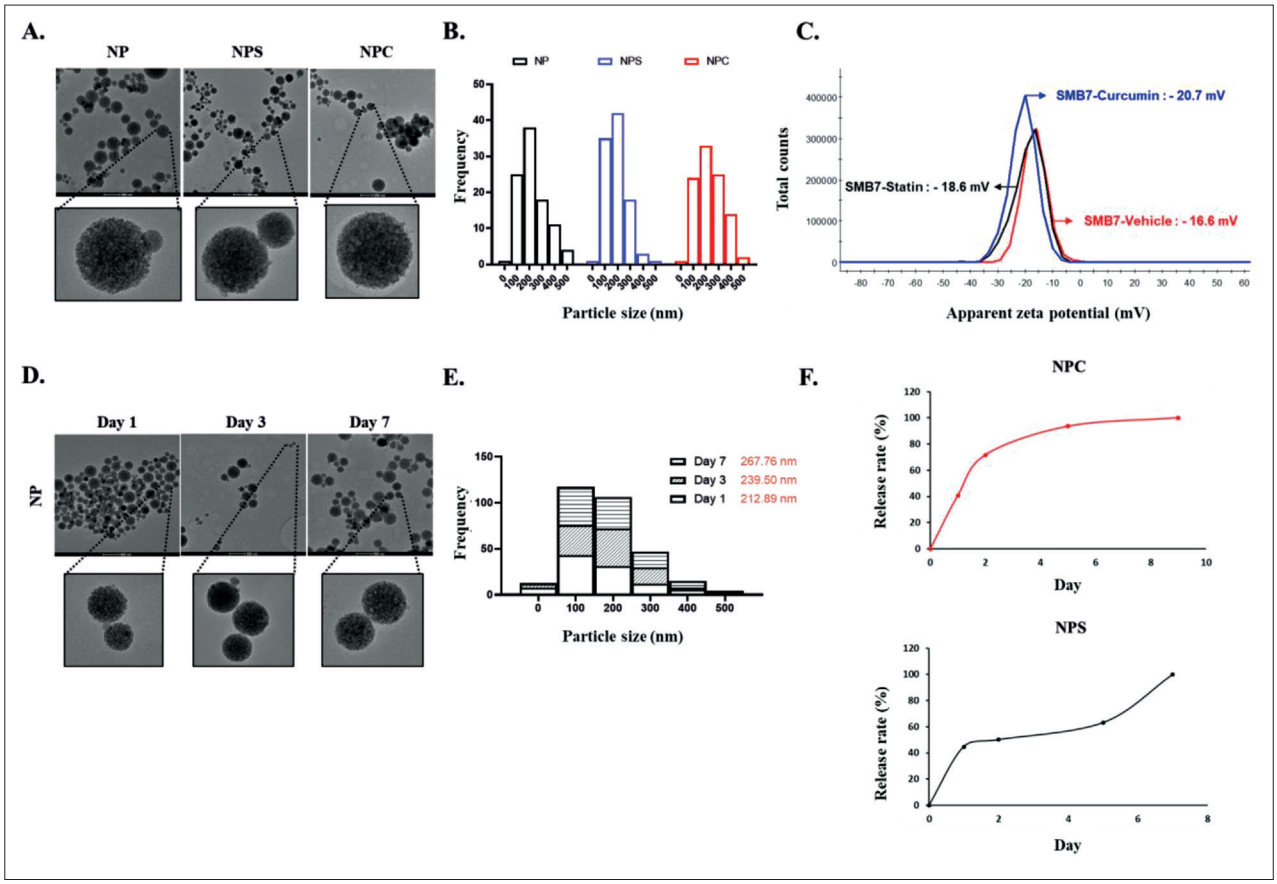

Figure 2. Characterization of statin- and curcumin-loaded nanoparticles. (A) Transmission electron microscopy (TEM) images of blank nanoparticles (NP), statin-loaded nanoparticles (NPS), and curcumin-loaded nanoparticles (NPC). (B) Size distribution graph displaying the measured size of each nanoparticle category. (C) Zeta potential analysis of NP, NPS, and NPC in phosphate-buffered saline (PBS; pH 7.4). (D) Storage stability study of NP, NPS, and NPC; size distribution was analyzed after samples were incubated for 1, 3, and 7 days at 37°C. (E) Size distribution graph displaying the measured size of each nanoparticle type after the samples were incubated for 1, 3, and 7 days at 37°C. (F) Cumulative release of statin and curcumin from nanoparticles assessed using liquid chromatography/mass spectrometry (LC/MS) analysis.

significantly increased upon treatment with NPSC. Curcumin is a type of antioxidant and can antagonize the deleterious effects of ROS. Intracellular ROS staining showed that the increased ROS level induced by hydrogen peroxide (H_2O_2) was suppressed in the NPSC group. To confirm whether the nanoparticles play a role in these effects, nanoparticles without being loaded with any of these drugs (NP) were administered (Figure 3J and K). The resistance to ROS was more pronounced in the NPSC-treated group than in the group treated with statin and curcumin.

3.3. 3D printing-based fabrication and characterization of nanoparticle-loaded artificial blood vessels

To ensure stable transplantation of nanoparticles and cells into the blood vessels, ABVs were fabricated by 3D printing (Figure 4A). The bioinks used in 3D printing (Figure 4B-i), the nozzles (Figure 4B-ii), and the printed ABVs (Figure 4B-iii) are briefly described. Artificial blood vessels, which can be customized in various sizes in terms of their external and internal diameters, can be 3D-printed as described (Figure 4C). Twenty-four hours after the fabrication of ABVs, a live/dead cell staining assay was conducted to verify the presence of cells within the luminal space of the vascular construct. In the case of blood vessels loaded with EPCs and NPS (EPC@NPS@BV), more cells were observed owing to the proliferative ability of the cells compared with the control group (EPC@NP@BV). Blood vessels loaded with EPCs and NPC (EPC@NPC@BV) were found to have a morphology similar to that of the controls. We found that the level of cell proliferation achieved in EPC@NPSC@BV was similar to that observed in NPS@BV (Figure 4D). The fabricated ABV was verified to contain intravascular cells within its internal structure. After we confirmed the presence of a vascular framework in the

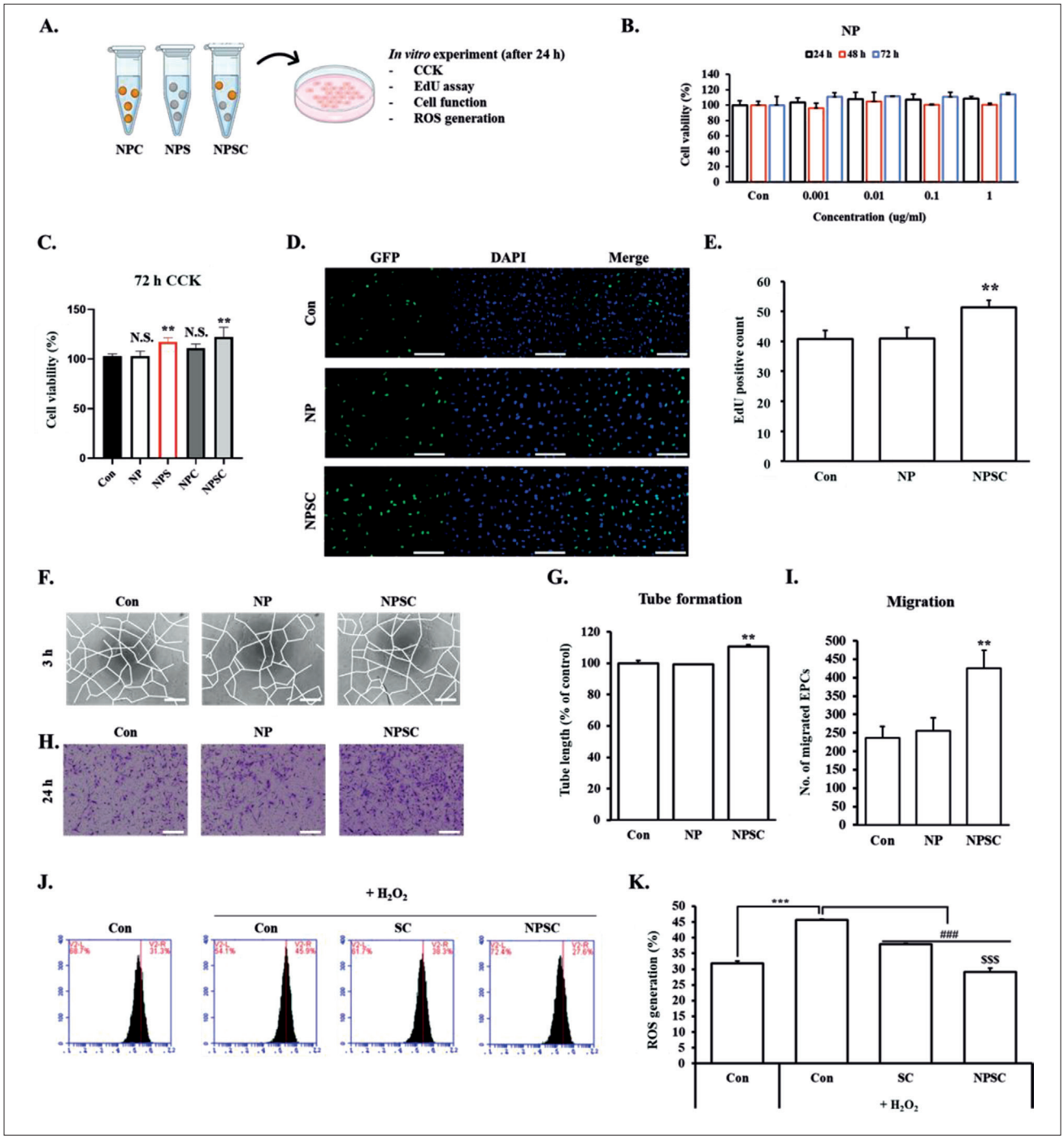

Figure 3. NPS and NPC improve the proliferation and antioxidant effect on EPCs. (A) Schematic illustration of *in vitro* experimental process for curcumin-loaded nanoparticles (NPC), statin-loaded nanoparticles (NPS), and nanoparticles-loaded statin and curcumin (NPSC). (B) EPCs viability in various concentration of blank nanoparticle (NP) ($N = 3$). (C) Cell viability after treatment with NP, NPS, NPC, and NPSC ($N = 3$). (D) Results of EdU cell proliferation assay; 200× magnification images ($N = 3$). Scale bars = 100 μm. (E) Quantification of EdU-positive cells. (F) Investigation of the tube-formation capacity of EPCs treated with NP and NPSC ($N = 3$). Scale bars = 50 μm. (G) Quantification of total tube length. (H) Investigation of the migration capacity of EPCs treated with NP and NPSC using Transwell migration assay. Scale bars = 50 μm. (I) Quantification of migrated cell. (J) ROS generation was measured using fluorescence-activated cell sorting (FACS) and 2′,7′-dichlorodihydrofluorescein diacetate (H_2DCFDA) ($N = 3$). (E) Quantification of the reactive oxygen species (ROS) generation rates using FACS data. Values are expressed as the mean ± standard derivation (SD). $^{*}p < 0.05$, $^{**}p < 0.01$, $^{***}p < 0.001$ as compared to the Con group (untreated group); $^{\#\#\#}p < 0.001$ as compared to the Con group with H_2O_2; $^{\$\$\$}p < 0.001$ as compared to the SC group (a group treated with statin and curcumin); N.S.: not significant.

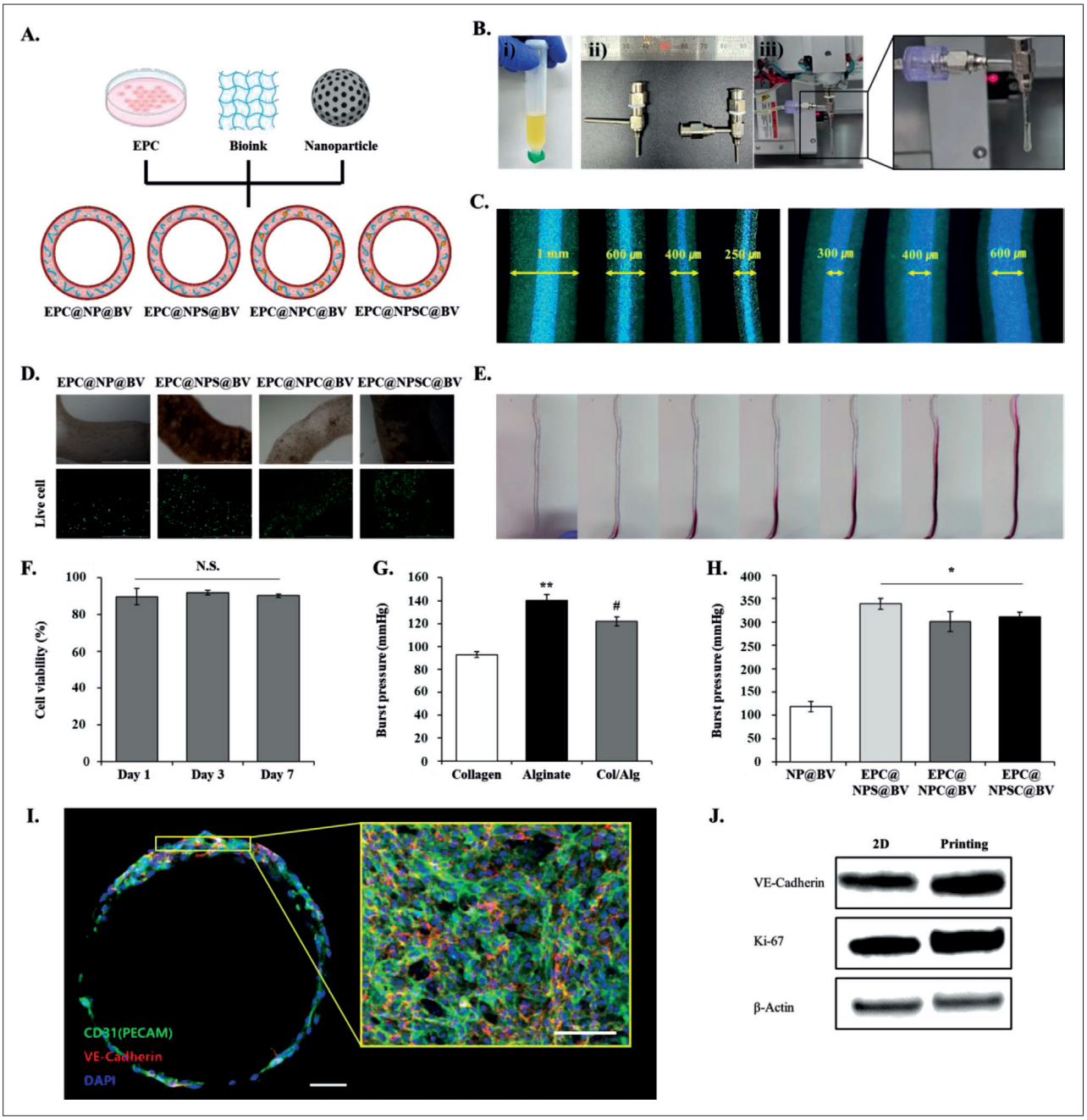

Figure 4. Characterization of 3D-printed artificial blood vessels (ABVs) loaded with endothelial progenitor cells (EPCs), statin-loaded nanoparticles (NPS), and curcumin-loaded nanoparticles (NPC). (A) Schematic illustration of 3D-printed process of ABVs with loaded EPCs and blank nanoparticles (NP), NPS, NPC, or nanoparticles loaded with statin and curcumin (NPSC). (B) Fabricating ABVs using bioink: (i) bioink, a material used in the 3D printing-based manufacture of ABVs; (ii) nozzles in different sizes; (iii) 3D printing of ABVs. (C) Microscopic images of 3D-printed ABVs containing two layers of different thicknesses, which is adjusted by using nozzles of different sizes. (D) Cell viability in groups treated with EPC@NP@BV (blood vessels loaded with EPC and nanoparticle), EPC@NPS@BV (blood vessels loaded with EPC and NPS), EPC@NPC@BV (blood vessels loaded with EPC and NPC), and EPC@NPSC@BV (blood vessels loaded with EPC, NPS, and NPC). (E) Fluidity of the 3D-printed ABVs. (F) Viability of EPCs loaded in ABV by 1, 3, and 7 days. NS indicates not statistically significant ($N = 3$). (G) Burst pressure of ABV fabricated with each bioink. $^{**}p < 0.01$ as compared to the collagen; $^{\#}p < 0.05$ as compared to the collagen ($N = 3$). (H) Burst pressure of ABV in each group NP@BV (NP-loaded blood vessel), EPC@NPS@BV, EPC@NPC@BV, and EPC@NPSC@BV on day 7 of culture. $^{*}p < 0.05$ as compared to the NP@BV ($N = 3$). (I) Expression of markers specific to EPCs, such as CD31 and VE-cadherin, in ABV was confirmed with immunofluorescence staining. (J) Western blotting of Ki-67 and VE-cadherin proteins in 2D-cultured EPCs (as "2D") and ABVs (as "printing").

fabricated ABV, we conducted an experiment to validate the blood flow through ABV, and verified that blood vessels were capable of reliable, sustained blood flow (Figure 4E). In addition to evaluating fluidity, we also investigated the impact of cell viability on blood vessel regeneration during the transplantation of cell-loaded ABV. Cell viability assessments were performed at multiple time points: 1, 3, and 7 days. The results demonstrated consistent and stable cell viability throughout the observation period, indicating the robustness of the cell-loaded ABVs in maintaining cell integrity and supporting potential tissue regeneration (Figure 4F). Further, mechanical properties of the vascular grafts such as burst pressure, compliance, and suture retention were evaluated.[25] In this study, ABVs made from alginate exhibited higher burst pressure values compared with those made solely from atelocollagen. However, due to the absence of cell adhesion ligands,[73] an ABV combining collagen and alginate was created to address the respective drawbacks of both materials (Figure 4G). Subsequently, burst pressure measurements were conducted to assess the burst pressure of cell-laden or cell-free ABVs, which were cultured for 7 days. The groups with cell-laden ABVs (i.e., EPC@NPS@BV, EPC@NPC@BV, EPC@NPSC@BV) exhibited an improvement in burst pressure of more than threefold compared to the cell-free ABV group (i.e., NP@BV) (Figure 4H). Next, to confirm continuous cell growth within the ABVs, fluorescence immunostaining was employed to assess the expression of essential EPC markers, such as CD31 and VE-cadherin (Figure 4I). Additionally, the protein-level expression of CD31 and Ki-67 was compared to that of two-dimensional (2D)-cultured EPCs. It is noteworthy that when transitioning from a 2D culture to a 3D culture environment, we observed a notable increase in the expression of endothelial cell-related markers (Figure 4J). This expression increase of these markers underscores the capacity of 3D culture systems in establishing a more physiologically relevant cellular environment. Unlike traditional 2D cultures, 3D cultures better mimic the natural microenvironment of cells within tissues and organs, allowing for improved cell–cell interactions and the formation of complex cell structures. In this context, the enhanced expression of endothelial cell-related markers suggests that our 3D culture model provides a more suitable platform for studying endothelial cell behavior and function.

3.4. *In vivo* transplantation of artificial blood vessels incorporating drugs-loaded nanoparticles in animal model

Based upon the aforementioned results, we conducted *in vivo* experiments to validate the effects of drugs encapsulated in nanoparticles. Furthermore, the stability of the 3D-printed ABVs incorporating cells and drug-loaded nanoparticles was assessed. The animal model of hindlimb ischemia created in this study was subjected to ABVs transplantation, and functional evaluation was performed (Figure 5A). When only PBS without cells or ABVs were transplanted, all hindlimbs of the treated animals were found to be necrotic. On the 14th day after transplantation, the group transplanted with ABVs without EPC or drug-loaded nanoparticles showed significant limb recovery (Figure 5B). During the follow-up period of up to 28 days, we found that the treatment effect was sustained, similar to that observed on the 14th day. Although the NP@BV group manifested excellent effect, the laser Doppler perfusion imaging results confirmed that the EPC@NPSC@BV group on day 14 showed more profound effect. Most importantly, the group transplanted with ABVs, together with cells and nanoparticles, showed the most pronounced effect from the 7th day after transplantation (Figure 5C). This strong therapeutic effect on the hindlimb was attributed to both the cells and ABVs. The efficacy of vascular endothelial cells is an important factor contributing to the recovery of hindlimb over time; however, EPC@NPSC@BV outperformed other counterparts in terms of the speed of recovery and the amount of blood flow during the recovery period. We also analyzed foot necrosis after transplantation (Figure 5D). Similar to the findings mentioned earlier, the highest incidence of necrosis was observed in the PBS and EPC groups. Notably, however, the EPC@NP@BV and EPC@NPSC@BV groups exhibited the most promising therapeutic outcomes, promoting limb recovery significantly faster than other groups (Figure 5E). This result is supported by the highest expression of α-SMA and CD31, which are vascular-related markers, observed in the EPC@NPSC@BV group (Figure 5F–I). In the final part of the experiment, we determined the presence of ROS generation within the tissue through DHE staining. We observed a significant reduction in DHE-positive staining in the EPC@NPSC@BV group, consistent with the staining results for markers associated with blood vessels (**Figure S2A** and **S2B** in Supplementary File). Taken together, these results collectively suggest the potential utility of ABVs incorporating drug-loaded nanoparticles and EPCs in mitigating the severity of ischemic diseases.

4. Discussion

Despite the advancements in drug therapy and surgical procedures for the treatment of vascular diseases, several notable disadvantages inherent in these approaches limit their long-term effectiveness. Drug therapy, while offering preventive benefits, often requires continuous administration, which may lead to side effects or drug resistance over time. Moreover, drug therapies may not

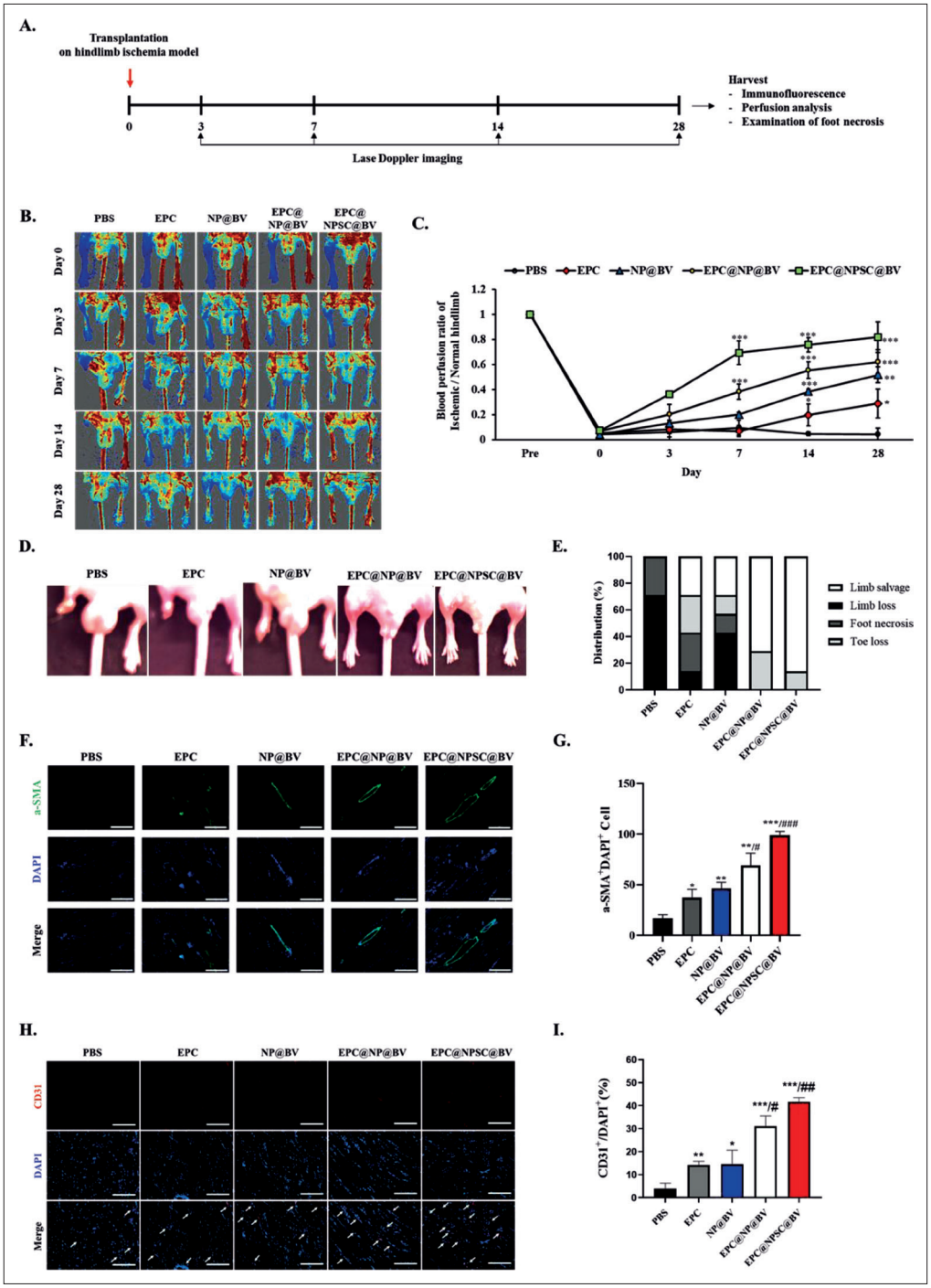

Figure 5. *In vivo* evaluation of 3D-bioprinted artificial blood vessels (ABVs) incorporating nanoparticles loaded with statin and curcumin (NPSC) in mouse model of hindlimb ischemia. (A) Schematic illustration of hindlimb ischemia model construction and ABV implantation. (B) The ratio of blood perfusion by laser Doppler imaging after phosphate-buffered saline (PBS), endothelial progenitor cells (EPC), NP@BV, EPC@NP@BV, and EPC@NPSC@BV transplantation in hindlimb ischemic model, created with BALB/c nude mice, at 0, 3, 7, 14, and 28 days post-transplantation. (C) Quantification of ratio of blood perfusion. (D) Necrosis at day 14 after ABV transplantation in a mouse model of hindlimb ischemia. (E) Quantification of necrosis. (F) Immunostaining with anti-α-smooth muscle actin (SMA) antibody (green) on ischemic limbs subjected to different treatments at 28 days post-transplantation. Scale bars = 200 μm. (G) Quantification of density of α-SMA-positive cells and DAPI-positive cells. (H) Immunostaining with anti-CD31 antibody (red) on ischemic limbs subjected to different treatments at 28 days post-plantation. Scale bars = 200 μm. (I) Quantification of density of CD31-positive cells and DAPI-positive cells. Values are expressed as mean ± standard deviation. $^{*}p < 0.05$; $^{**}p < 0.01$ versus PBS. $^{\#}p < 0.05$, $^{\#\#}p < 0.01$, $^{\#\#\#}p < 0.001$ versus NP.

be able to comprehensively address the underlying causes of vascular diseases, and their efficacy can vary among individuals.[74-76] Contrarily, surgical interventions such as the use of stents or catheters can provide immediate relief by improving blood flow. However, they can be associated with complications, including restenosis or blood clot formation, which may necessitate additional procedures. Additionally, some patients may not be suitable candidates for invasive surgery because of their underlying health conditions or anatomical complexities.[77-79] To overcome the limitations of traditional drug therapy and surgical procedures, this study was designed to leverage innovative approaches combining the strengths of nanotechnology, 3D printing, and cell therapies.

A key aspect addressed in these *in vivo* studies is the microenvironment of the implantation site, which plays a crucial role in determining the success of ABV transplantation. The ROS or hypoxic environment at the transplant site poses a challenge for the transplanted cells to adapt effectively.[54-56] To surmount this limitation, the use of curcumin, known for its antioxidant and anti-inflammatory properties, has been employed to aid cell adaptation to the microenvironment.[57-59] Additionally, the incorporation of statins, renowned for their cardiovascular protective effects, has been explored to enhance cell function and improve treatment efficacy. Nanotechnology plays a pivotal role in optimizing drug delivery.[60-62] Encapsulating statins and curcumin within nanoparticles exhibit several advantages, including enhanced bioavailability, controlled release, and targeted delivery to specific sites.[65-67] This study aimed to improve the efficacy in vascular disease treatment by employing ABVs loaded with nanoparticles and cells. The use of nanoparticles encapsulating therapeutic substances such as statin and curcumin enables controlled and targeted drug delivery, minimizes potential side effects, and ensures sustained drug release over time. The incorporation of stem cells into ABVs promotes angiogenesis and offers a promising avenue to repair damaged blood vessels more effectively. The 3D printing technology allows for precise fabrication of ABVs tailored to individual patient needs, thereby improving the success rate and adaptability of the intervention. By combining these advanced techniques, the experiment sought to optimize treatment delivery and efficacy with the ultimate goal of addressing the fundamental challenges of vascular diseases and enhancing patient outcomes in the long run.

This study demonstrated the successful fabrication and characterization of statin- and curcumin-loaded nanoparticles (NPS and NPC, respectively) and their potential applications in vascular regeneration. These results highlight several important aspects, including the properties of the nanoparticles, their biocompatibility, and their therapeutic effects both *in vitro* and *in vivo*. The fabrication process yielded nanoparticles with consistent spherical shapes and sizes, indicating the reproducibility and stability of the manufacturing method. The sustained release profiles of the loaded drugs from the nanoparticles suggest their potential for use in controlled and prolonged drug delivery, which is crucial for therapeutic interventions (Figure 2). A biocompatibility assessment revealed that the nanoparticles exhibited no cytotoxic effects, even at high concentrations, over an extended period (Figure 3B and C). This finding is crucial for their safe application in biomedical settings. While nanoparticle release is gradual, the resulting biological responses exhibit significant variability, primarily depending on nanoparticle properties and the specific target tissue. We have consistently observed that when cells are directly treated with nanoparticles, cell proliferation, migration, and tube formation are significantly improved due to cellular uptake (Figure 3D–I). However, our study extended beyond this initial timeframe, meticulously examining the sustained and gradual release kinetics of these nanoparticles (Figure 2F). It accomplishes this by ensuring a continuous and steady supply of bioactive agents, which, in turn, supports various aspects of tissue healing and recovery processes over an extended duration. These results suggest that nanoparticles can enhance the regenerative potential of EPCs, which is vital for vascular repair and angiogenesis. The co-administration of NPS and NPC (NPSC) further augmented the therapeutic effects of the nanoparticles (Figure 3J and K). Curcumin, known for its antioxidant properties, reduces the levels of intracellular ROS induced by H_2O_2, thereby providing additional protection against oxidative stress. We have substantiated these effects through additional *in vivo* experiments (**Figure S2A** and **S2B** in Supplementary File). This finding highlights the potential of combining multiple therapeutic agents within a single nanoparticle delivery system to achieve synergistic effects. The controlled release of therapeutic agents, along with the demonstrated biocompatibility, enhanced cell proliferation, and angiogenic properties of the nanoparticles, highlights that combining them with nanoparticles is a compelling approach for applications in tissue engineering and regenerative medicine. Furthermore, this study reveals the plausibility of utilizing dual drugs to enhance the efficacy of vascular regeneration as compared to a single drug, as demonstrated in our previous study.[68] This study showcases the synergistic effect of both statin and curcumin, with the former wielding a prominent influence in regeneration and the latter regulating the microenvironment. This suggests

that the simultaneous administration of multiple drugs, as opposed to the introduction of a single agent, may contribute to a synergistic effect, thereby facilitating the treatment of ischemic diseases. Further research and optimization of nanoparticle delivery systems are warranted to fully understand their mechanisms of action and explore their clinical potential.

The successful fabrication of nanoparticle-laden ABVs using 3D printing technology is a significant advancement in the field of tissue engineering. The ability to create ABVs with customizable sizes and integrated nanoparticles opens new possibilities for targeted drug delivery and localized therapy (Figure 4). The preserved viability and proliferative capacity of cells within ABVs indicate their potential for supporting vascular regeneration. In the *in vivo* transplantation experiment, necrosis was observed in the control group that received ABVs without cells or nanoparticles, highlighting the importance of utilizing combination therapy encompassing cells and drugs. However, the groups that received ABVs loaded with cells and nanoparticles exhibited remarkable recovery from hindlimb ischemia. At 28 days, the EPC@NP@BV group exhibited significantly pronounced vascular recovery ability, whereas the EPC@NPSC@BV group attained the fastest recovery, marked by almost complete recovery within 14 days. The EPC@NPSC@BV group demonstrated the most significant improvements in terms of recovery speed and blood flow, attesting to the synergistic effects of statin and curcumin in cell-based therapy (Figure 5B–E). These findings suggest that EPCs enhance their functionality and proliferative capacity through the uptake of therapeutic agents, thus assuming a critical role in facilitating vascular recovery subsequent to ABV transplantation (Figure 3). Histological analysis revealing enhanced expression of vascular-related markers, such as α-SMA and CD31, in the EPC@NPSC@BV group further supported these outcomes (Figure 5F–I). These findings point to the capability of the combination therapy in facilitating the regeneration of functional blood vessels, which leads to improved angiogenesis.

5. Conclusion

In this study, we successfully prepared NPS and NPC, which were in consistent spherical shape and demonstrate sustained release profiles. The nanoparticles exhibited excellent biocompatibility and promoted the proliferative capacity and functionality of EPC. The integration of these nanoparticles within ABVs using 3D printing technology allows for customizable and functional constructs capable of promoting vascular regeneration. In *in vivo* models, the transplantation of nanoparticle-loaded ABVs resulted in significant improvements in hindlimb ischemia, marked by enhanced recovery speed and blood flow. These findings highlight the potential of statin- and curcumin-loaded nanoparticles as a promising approach for controlled drug delivery and regeneration of functional blood vessels. Further research and optimization are required to fully explore their clinical potential and pave the way for future therapeutic applications.

Acknowledgments

None.

Funding

This work was supported by a grant from the National Research Foundation (NRF2020R1A2C2101297 and 2022R1A5A2027161) funded by the Korean government.

Conflict of interest

The authors declare no conflicts of interest.

Author contributions

Conceptualization: Eun Ji Lee, Jaewoo Choi, Woong Bi Jang, Sang-Mo Kwon

Formal analysis: Eun Ji Lee, Jaewoo Choi, Woong Bi Jang

Investigation: Eun Ji Lee, Jaewoo Choi, Woong Bi Jang, Hye Ji Lim

Methodology: Eun Ji Lee, Jaewoo Choi, Woong Bi Jang, Hye Ji Lim, Deokhyeon Yoon, Dong Myoung Lee, Donggu Kang, Jeong-Seok Lee, Hojun Jeon, Kyeong Hyeon Lee, Yong-Il Shin, Sang-Cheol Han

Writing – original draft: Eun Ji Lee, Jaewoo Choi, Woong Bi Jang

Writing – review & editing: Sang-Mo Kwon

Ethics approval and consent to participate

Human umbilical cord blood was collected from healthy volunteers after obtaining informed consent according to the protocol approved by the Institutional Review Board of Pusan National University Yangsan Hospital, Republic of Korea (Approval No. PNUYH-05-2017-053). Animal treatment and maintenance were performed in accordance with the Principles of Laboratory Animal Care, and animal experiments were performed in accordance with protocols approved by the Pusan National University Institutional Animal Use and Care Committee (Approval No. PNU-2022-0212).

Consent for publication

In accordance with the guidelines for publication involving human subjects, we obtained written consent from

all participants included in our study. Any identifying information has been appropriately masked to protect the privacy of the patients. We have made every effort to adhere to the consent and privacy guidelines set forth. Therefore, this requirement is applicable and has been fulfilled.

Availability of data

The data utilized in this study are available from the corresponding author (Sang-Mo Kwon, Email: smkwon323@pusan.ac.kr) upon reasonable request.

References

1. Pancholy SB, Patel GA, Shah SC, Patel TM. Vascular complications of the wrist: prevention and management. *Interv Cardiol Clin*. 2020;9(1):87-97. doi: 10.1016/j.iccl.2019.08.002
2. Fan J, Watanabe T. Atherosclerosis: known and unknown. *Pathol Int*. 2022;72(3):151-160. doi: 10.1111/pin.13202
3. Libby P. The changing landscape of atherosclerosis. *Nature*. 2021;592(7855):524-533. doi: 10.1038/s41586-021-03392-8
4. Balta S. Endothelial dysfunction and inflammatory markers of vascular disease. *Curr Vasc Pharmacol*. 2021;19(3):243-249. doi: 10.2174/1570161118666200421142542
5. Han Y, Li L, Zhang Y, et al. Phenomics of vascular disease: the systematic approach to the combination therapy. *Curr Vasc Pharmacol*. 2015;13(4):433-440. doi: 10.2174/1570161112666141014144829
6. Horvath L, Nemeth N, Feher G, Kívés Z, Endrei D, Boncz I. Epidemiology of peripheral artery disease: narrative review. *Life (Basel)*. 2022;12(7):1041. doi: 10.3390/life12071041
7. St Hilaire C. Medial arterial calcification: a significant and independent contributor of peripheral artery disease. *Arterioscler Thromb Vasc Biol*. 2022;42(3):253-260. doi: 10.1161/ATVBAHA.121.316252
8. Conte SM, Vale PR. Peripheral arterial disease. *Heart Lung Circ*. 2018;27(4):427-432. doi: 10.1016/j.hlc.2017.10.014
9. Regmi M, Siccardi MA. *Coronary Artery Disease Prevention*. Treasure Island, FL: StatPearls; 2023.
10. Pragodpol P, Ryan C. Critical review of factors predicting health-related quality of life in newly diagnosed coronary artery disease patients. *J Cardiovasc Nurs*. 2013;28(3):277-284. doi: 10.1097/JCN.0b013e31824af56e
11. Lichota A, Szewczyk EM, Gwozdzinski K. Factors affecting the formation and treatment of thrombosis by natural and synthetic compounds. *Int J Mol Sci*. 2020;21(21):7975. doi: 10.3390/ijms21217975
12. Chen H, McGowan EM, Ren N, et al. Nattokinase: a promising alternative in prevention and treatment of cardiovascular diseases. *Biomark Insights*. 2018;13:1177271918785130. doi: 10.1177/1177271918785130
13. Krisnanda C, Menahem S, Lane GK. Intravascular stent implantation for the management of pulmonary artery stenosis. *Heart Lung Circ*. 2013;22(1):56-70. doi: 10.1016/j.hlc.2012.08.008
14. Elens M, Le Fevere de Ten Hove G. In stent re-stenosis after carotid artery stenting. *Eur J Vasc Endovasc Surg*. 2023;65(3):378. doi: 10.1016/j.ejvs.2022.11.026
15. John S, Bain MD, Hui FK, et al. Long-term follow-up of in-stent stenosis after pipeline flow diversion treatment of intracranial aneurysms. *Neurosurgery*. 2016;78(6):862-867. doi: 10.1227/NEU.0000000000001146
16. Chiarito M, Mehran R. Panta rhei, also drug eluting stent technology. *Catheter Cardiovasc Interv*. 2020;95(6):1074-1075. doi: 10.1002/ccd.28918
17. El-Kadiry AE, Rafei M, Shammaa R. Cell therapy: types, regulation, and clinical benefits. *Front Med (Lausanne)*. 2021;8:756029. doi: 10.3389/fmed.2021.756029
18. Zhang L, Xu Q. Stem/progenitor cells in vascular regeneration. *Arterioscler Thromb Vasc Biol*. 2014;34(6):1114-1119. doi: 10.1161/ATVBAHA.114.303809
19. Zakrzewski W, Dobrzynski M, Szymonowicz M, Rybak Z. Stem cells: past, present, and future. *Stem Cell Res Ther*. 2019;10(1):68. doi: 10.1186/s13287-019-1165-5
20. Xie Y, Fan Y, Xu Q. Vascular regeneration by stem/progenitor cells. *Arterioscler Thromb Vasc Biol*. 2016;36(5):e33-40. doi: 10.1161/ATVBAHA.116.307303
21. Leeper NJ, Hunter AL, Cooke JP. Stem cell therapy for vascular regeneration: adult, embryonic, and induced pluripotent stem cells. *Circulation*. 122(5):517-526. doi: 10.1161/CIRCULATIONAHA.109.881441
22. Bashor CJ, Hilton IB, Bandukwala H, Smith DM, Veiseh O. Engineering the next generation of cell-based therapeutics. *Nat Rev Drug Discov*. 2022;21(9):655-675. doi: 10.1038/s41573-022-00476-6
23. Lovell MJ, Mathur A. Cardiac stem cell therapy: progress from the bench to bedside. *Heart*. 2010;96(19):1531-1537. doi: 10.1136/hrt.2009.192385
24. Hou YC, Cui X, Qin Z, et al. Three-dimensional bioprinting of artificial blood vessel: process, bioinks, and challenges. *Int J Bioprint*. 2023;9(4):740. doi: 10.18063/ijb.740
25. Yang GH, Kang D, An S, et al. Advances in the development of tubular structures using extrusion-based 3D cell-printing technology for vascular tissue regenerative applications. *Biomater Res*. 2022;26(1):73. doi: 10.1186/s40824-022-00321-2

26. Moore MJ, Tan RP, Yang N, Rnjak-Kovacina J, Wise SG. Bioengineering artificial blood vessels from natural materials. *Trends Biotechnol*. 2022;40(6):693-707. doi: 10.1016/j.tibtech.2021.11.003

27. Wang D, Xu Y, Li Q, Turng L-S. Artificial small-diameter blood vessels: materials, fabrication, surface modification, mechanical properties, and bioactive functionalities. *J Mater Chem B*. 2020;8(9):1801-1822. doi: 10.1039/c9tb01849b

28. Sun D, Zheng Y, Yin T, et al. Coronary drug-eluting stents: from design optimization to newer strategies. *J Biomed Mater Res A*. 2014;102(5):1625-40. doi: 10.1002/jbm.a.34806

29. Sternberg K, Grabow N, Petersen S, et al. Advances in coronary stent technology--active drug-loaded stent surfaces for prevention of restenosis and improvement of biocompatibility. *Curr Pharm Biotechnol*. 2013;14(1):76-90. doi: 10.2174/138920113804805377

30. Wang Z, Lee SJ, Cheng HJ, Yoo JJ, Atala A. 3D bioprinted functional and contractile cardiac tissue constructs. *Acta Biomater*. 2018;70:48-56. doi: 10.1016/j.actbio.2018.02.007

31. Neumann B, Baror R, Zhao C, et al. Metformin restores CNS remyelination capacity by rejuvenating aged stem cells. *Cell Stem Cell*. 2019;25(4):473-485.e8. doi: 10.1016/j.stem.2019.08.015

32. Jang WB, Park JH, Ji ST, et al. Cytoprotective roles of a novel compound, MHY-1684, against hyperglycemia-induced oxidative stress and mitochondrial dysfunction in human cardiac progenitor cells. *Oxid Med Cell Longev*. 2018;2018:4528184. doi: 10.1155/2018/4528184

33. Mohseni N, Roshan R, Naderi S, Behdani M, Kazemi-Lomedasht F. In vitro combination therapy of pathologic angiogenesis using anti-vascular endothelial growth factor and anti-neuropilin-1 nanobodies. *Iran J Basic Med Sci*. 2020;23(10):1335-1339. doi: 10.22038/ijbms.2020.47782.11000

34. Niklason LE, Lawson JH. Bioengineered human blood vessels. *Science*. 2020;370(6513):eaaw8682. doi: 10.1126/science.aaw8682

35. Papaioannou TG, Manolesou D, Dimakakos E, Tsoucalas G, Vavuranakis M, Tousoulis D. 3D bioprinting methods and techniques: applications on artificial blood vessel fabrication. *Acta Cardiol Sin*. 2019;35(3):284-289. doi: 10.6515/ACS.201905_35(3).20181115A

36. Kakisis JD, Liapis CD, Breuer C, Sumpio BE. Artificial blood vessel: the Holy Grail of peripheral vascular surgery. *J Vasc Surg*. 2005;41(2):349-354. doi: 10.1016/j.jvs.2004.12.026

37. Colosi C, Shin SR, Manoharan V, et al. Microfluidic bioprinting of heterogeneous 3D tissue constructs using low-viscosity bioink. *Adv Mater*. 2016;28(4):677-684. doi: 10.1002/adma.201503310

38. Munisso MC, Yamaoka T. Circulating endothelial progenitor cells in small-diameter artificial blood vessel. *J Artif Organs*. 2020;23(1):6-13. doi: 10.1007/s10047-019-01114-6

39. Zhou X, Nowicki M, Sun H, et al. 3D bioprinting-tunable small-diameter blood vessels with biomimetic biphasic cell layers. *ACS Appl Mater Interfaces*. 2020;12(41):45904-45915. doi: 10.1021/acsami.0c14871

40. Lee A, Hudson AR, Shiwarski DJ, et al. 3D bioprinting of collagen to rebuild components of the human heart. *Science*. 2019;365(6452):482-487. doi: 10.1126/science.aav9051

41. Alonzo M, AnilKumar S, Roman B, Tasnim N, Joddar B. 3D bioprinting of cardiac tissue and cardiac stem cell therapy. *Transl Res*. 2019;211:64-83. doi: 10.1016/j.trsl.2019.04.004

42. Mazzocchi A, Soker S, Skardal A. 3D bioprinting for high-throughput screening: drug screening, disease modeling, and precision medicine applications. *Appl Phys Rev*. 2019;6(1):011302. doi: 10.1063/1.5056188

43. Vanderburgh J, Sterling JA, Guelcher SA. 3D printing of tissue engineered constructs for in vitro modeling of disease progression and drug screening. *Ann Biomed Eng*. 2017;45(1):164-179. doi: 10.1007/s10439-016-1640-4

44. Gonzalez LM, Moeser AJ, Blikslager AT. Animal models of ischemia-reperfusion-induced intestinal injury: progress and promise for translational research. *Am J Physiol Gastrointest Liver Physiol*. 2015;308(2):G63-75. doi: 10.1152/ajpgi.00112.2013

45. Rahbar Saadat Y, Hosseiniyan Khatibi SM, Sani A, Vahed SZ, Ardalan M. Ischemic tubular injury: oxygen-sensitive signals and metabolic reprogramming. *Inflammopharmacology*. 2023;31(4):1657-1669. doi: 10.1007/s10787-023-01232-x

46. Guan Y, Gao N, Niu H, Dang Y, Guan J. Oxygen-release microspheres capable of releasing oxygen in response to environmental oxygen level to improve stem cell survival and tissue regeneration in ischemic hindlimbs. *J Control Release*. 2021;331:376-389. doi: 10.1016/j.jconrel.2021.01.034

47. Dambrova M, Zuurbier CJ, Borutaite V, Liepinsh E, Makrecka-Kuka M. Energy substrate metabolism and mitochondrial oxidative stress in cardiac ischemia/reperfusion injury. *Free Radic Biol Med*. 2021;165:24-37. doi: 10.1016/j.freeradbiomed.2021.01.036

48. Rojas-Morales P, Leon-Contreras JC, Sanchez-Tapia M, et al. A ketogenic diet attenuates acute and chronic ischemic kidney injury and reduces markers of oxidative stress and inflammation. *Life Sci*. 2022;289:120227. doi: 10.1016/j.lfs.2021.120227

49. Mokhtari-Zaer A, Marefati N, Atkin SL, Butler AE, Sahebkar A. The protective role of curcumin in myocardial ischemia-reperfusion injury. *J Cell Physiol*. 2018;234(1):214-222. doi: 10.1002/jcp.26848

50. Malko P, Jiang LH. TRPM2 channel-mediated cell death: an important mechanism linking oxidative stress-inducing pathological factors to associated pathological conditions. *Redox Biol*. 2020;37:101755. doi: 10.1016/j.redox.2020.101755

51. Zhao X, Li S, Mo Y, et al. DCA protects against oxidation injury attributed to cerebral ischemia-reperfusion by regulating glycolysis through PDK2-PDH-Nrf2 axis. *Oxid Med Cell Longev*. 2021;2021:5173035. doi: 10.1155/2021/5173035

52. Rivera JC, Dabouz R, Noueihed B, Omri S, Tahiri H, Chemtob S. Ischemic retinopathies: oxidative stress and inflammation. *Oxid Med Cell Longev*. 2017;2017:3940241. doi: 10.1155/2017/3940241

53. Santos-Zas I, Lemarie J, Tedgui A, Ait-Oufella H. Adaptive immune responses contribute to post-ischemic cardiac remodeling. *Front Cardiovasc Med*. 2018;5:198. doi: 10.3389/fcvm.2018.00198

54. Carlsson PO. Influence of microenvironment on engraftment of transplanted beta-cells. *Ups J Med Sci*. 2011;116(1):1-7. doi: 10.3109/03009734.2010.548609

55. Yan LL, Ye LP, Chen YH, et al. The influence of microenvironment on survival of intraportal transplanted islets. *Front Immunol*. 2022;13:849580. doi: 10.3389/fimmu.2022.849580

56. Zenclussen AC, Hammerling GJ. Cellular regulation of the uterine microenvironment that enables embryo implantation. *Front Immunol*. 2015;6:321. doi: 10.3389/fimmu.2015.00321

57. Yavarpour-Bali H, Ghasemi-Kasman M, Pirzadeh M. Curcumin-loaded nanoparticles: a novel therapeutic strategy in treatment of central nervous system disorders. *Int J Nanomedicine*. 2019;14:4449-4460. doi: 10.2147/IJN.S208332

58. Abrahams S, Haylett WL, Johnson G, Carr JA, Bardien S. Antioxidant effects of curcumin in models of neurodegeneration, aging, oxidative and nitrosative stress: a review. *Neuroscience*. 2019;406:1-21. doi: 10.1016/j.neuroscience.2019.02.020

59. Patel SS, Acharya A, Ray RS, Agrawal R, Raghuwanshi R, Jain P. Cellular and molecular mechanisms of curcumin in prevention and treatment of disease. *Crit Rev Food Sci Nutr*. 2020;60(6):887-939. doi: 10.1080/10408398.2018.1552244

60. Zhao W, Xiao ZJ, Zhao SP. The benefits and risks of statin therapy in ischemic stroke: a review of the literature. *Neurol India*. 2019;67(4):983-992. doi: 10.4103/0028-3886.266274

61. Stancu C, Sima A. Statins: mechanism of action and effects. *J Cell Mol Med*. 2001;5(4):378-387. doi: 10.1111/j.1582-4934.2001.tb00172.x

62. Lee SE, Chang HJ, Sung JM, et al. Effects of statins on coronary atherosclerotic plaques: the PARADIGM Study. *JACC Cardiovasc Imaging*. 2018;11(10):1475-1484. doi: 10.1016/j.jcmg.2018.04.015

63. Hoshyar N, Gray S, Han H, Bao G. The effect of nanoparticle size on in vivo pharmacokinetics and cellular interaction. *Nanomedicine (Lond)*. 2016;11(6):673-692. doi: 10.2217/nnm.16.5

64. Zhang S, Gao H, Bao G. Physical principles of nanoparticle cellular endocytosis. *ACS Nano*. 2015;9(9):8655-8671. doi: 10.1021/acsnano.5b03184

65. Suk JS, Xu Q, Kim N, Hanes J, Ensign LM. PEGylation as a strategy for improving nanoparticle-based drug and gene delivery. *Adv Drug Deliv Rev*. 2016;99(Pt A):28-51. doi: 10.1016/j.addr.2015.09.012

66. Saraiva C, Praca C, Ferreira R, Santos T, Ferreira L, Bernardino L. Nanoparticle-mediated brain drug delivery: overcoming blood-brain barrier to treat neurodegenerative diseases. *J Control Release*. 2016;235:34-47. doi: 10.1016/j.jconrel.2016.05.044

67. Donahue ND, Acar H, Wilhelm S. Concepts of nanoparticle cellular uptake, intracellular trafficking, and kinetics in nanomedicine. *Adv Drug Deliv Rev*. 2019;143:68-96. doi: 10.1016/j.addr.2019.04.008

68. Gao G, Lee JH, Jang J, et al. Tissue engineered bio-blood-vessels constructed using a tissue-specific bioink and 3d coaxial cell printing technique: a novel therapy for ischemic disease. *Adv Funct Mater*. 2017;27(33):1700798. doi: 10.1002/adfm.201770192

69. Kim J, Kim HS, Lee N, et al. Multifunctional uniform nanoparticles composed of a magnetite nanocrystal core and a mesoporous silica shell for magnetic resonance and fluorescence imaging and for drug delivery. *Angew Chem Int Ed Engl*. 2008;47(44):8438-8441. doi: 10.1002/anie.200802469

70. Lee SH, Lee JH, Yoo SY, Hur J, Kim H-S, Kwon SM. Hypoxia inhibits cellular senescence to restore the therapeutic potential of old human endothelial progenitor cells via the hypoxia-inducible factor-1alpha-TWIST-p21 axis. *Arterioscler Thromb Vasc Biol*. 2013;33(10):2407-2414. doi: 10.1161/ATVBAHA.113.301931

71. Guo X, Mao F, Wang W, Yang Y, Bai Z. Sulfhydryl-modified Fe3O4@SiO2 core/shell nanocomposite: synthesis and toxicity assessment in vitro. *ACS Appl Mater Interfaces*. 2015;7(27):14983-14991. doi: 10.1021/acsami.5b03873

72. Shi B, Xie L, Ma B, Zhou Z, Xu B, Qu L. Preparation and properties of highly transparent SiO(2) aerogels for thermal insulation. *Gels*. 2022;8(11):744.
doi: 10.3390/gels8110744

73. Gheorghita Puscaselu R, Lobiuc A, Dimian M, Covasa M. Alginate: from food industry to biomedical applications and management of metabolic disorders. *Polymers (Basel)*. 2020;12(10):2417.
doi: 10.3390/polym12102417

74. Tarbell JM, Cancel LM. The glycocalyx and its significance in human medicine. *J Intern Med*. 2016;280(1):97-113.
doi: 10.1111/joim.12465

75. Schmelzer KP, Liebetrau D, Kammerer W, Meisinger C, Hyhlik-Dürr A. Strategies for avoiding typical drug-drug interactions and drug-related problems in patients with vascular diseases. *Medicina (Kaunas)*. 2023; 59(4):780.
doi: 10.3390/medicina59040780

76. Huynh DTN, Heo KS. Therapeutic targets for endothelial dysfunction in vascular diseases. *Arch Pharm Res*. 2019;42(10):848-861.
doi: 10.1007/s12272-019-01180-7

77. Weiss AJ, Lorente-Ros M, Correa A, Barman N, Tamis-Holland JE. Recent advances in stent technology: do they reduce cardiovascular events? *Curr Atheroscler Rep*. 2022;24(9):731-744.
doi: 10.1007/s11883-022-01049-z

78. Suryawan IGR, Luke K, Agustianto RF, Budi Mulia EP. Coronary stent infection: a systematic review. *Coron Artery Dis*. 2022;33(4):318-326.
doi: 10.1097/MCA.0000000000001098

79. Sanchez-Jimenez E, El-Mokdad R, Chaddad R, Cortese B. Drug-coated balloon for the management of coronary chronic total occlusions. *Rev Cardiovasc Med*. 2022;23(2):42.
doi: 10.31083/j.rcm2302042